

The vortex gas scaling regime of baroclinic turbulence

Basile Gallet^{a,1} and Raffaele Ferrari^b

^aService de Physique de l'Etat Condensé, CEA Saclay, CNRS UMR 3680, Université Paris-Saclay, 91191 Gif-sur-Yvette, France.; ^bMassachusetts Institute of Technology, USA

This manuscript was compiled on December 23, 2019

1 **The mean state of the atmosphere and ocean is set through a balance**
2 **between external forcing – radiative processes in the atmosphere**
3 **and air-sea fluxes of momentum, heat and freshwater in the ocean**
4 **– and the emergent turbulence which transfers energy to dissipative**
5 **structures, primarily through friction in bottom boundary layers. The**
6 **external forcing maintains lateral temperature gradients, which on**
7 **a rotating planet give rise to flows along the temperature contours:**
8 **jets in the atmosphere and currents in the ocean. These large-scale**
9 **flows spontaneously develop turbulent eddies through the baroclinic**
10 **instability. A critical step in the development of a theory of climate is**
11 **to properly include the resulting eddy-induced turbulent transport of**
12 **properties like heat, moisture, and carbon. In the early linear stages,**
13 **baroclinic instability generates flow structures at the Rossby deformation**
14 **radius, a length scale of order 1000 km in the atmosphere**
15 **and 100 km in the ocean, smaller than the planetary scale and much**
16 **smaller than the typical extent of ocean basins respectively. There is**
17 **therefore a separation of scales, arguably more in the ocean than in**
18 **the atmosphere, between the large-scale temperature gradient and**
19 **the smaller eddies that advect it randomly, inducing effective diffusion.**
20 **Numerical solutions of the two-layer quasi-geostrophic model,**
21 **the standard model for studies of eddy motions in the atmosphere**
22 **and ocean, show that such scale separation remains in the strongly**
23 **nonlinear turbulent regime, provided there is sufficient bottom drag.**
24 **We compute the scaling-laws governing the eddy-driven transport**
25 **associated with baroclinic turbulence. First, we provide a theoretical**
26 **underpinning for empirical scaling-laws reported in previous studies,**
27 **for different formulations of the bottom drag law. Secondly, these**
28 **scaling-laws are shown to provide an important first step toward an**
29 **accurate local closure to predict the impact of baroclinic turbulence**
30 **in setting the large-scale temperature profiles in the atmosphere and**
31 **ocean.**

Oceanography | Atmospheric dynamics | Turbulence

1 **O**ceanic and atmospheric flows are subject to the combined effects of strong density stratification and rapid planetary rotation. On the one hand, these two ingredients add complexity to the dynamics, making the flow strongly anisotropic and inducing waves that modify the characteristics of the turbulent eddies. On the other hand, they permit the derivation of reduced sets of equations that capture the large-scale behavior of the flow: this is the realm of quasi-geostrophy (QG). The outcome of this approach is a model that couples two-dimensional layers of fluid of different density. QG filters out fast-wave dynamics, relaxing the necessity to resolve the fastest time scales of the original system. A QG model with only two fluid layers is simple enough for fast and extensive numerical studies, and yet it retains the key phenomenon arising from the combination of stable stratification and rapid rotation (1): baroclinic instability, with its ability to induce small-scale turbulent eddies from a large-scale ver-

18 tically sheared flow. The two-layer quasi-geostrophic model (2LQG) offers a testbed to derive and validate closure models for the “baroclinic turbulence” that results from this instability. 19 20 21

22 In the simplest picture of 2LQG, a layer of light fluid sits on top of a layer of heavy fluid, as sketched in Fig. 1a, in a frame rotating at a spatially uniform rate $\Omega = f/2$ around the vertical axis. Such a uniform Coriolis parameter f is a strong simplification as compared to real atmospheres and oceans, where the β -effect associated with latitudinal variations in f can trigger the emergence of zonal jets. Nevertheless, β vanishes at the poles of a planet, and it seems that any global parameterization of baroclinic turbulence needs to correctly handle the limiting case $\beta = 0$, which we address in the present study. The 2LQG model applies to motions evolving on timescales long compared to the planetary rotation – the small-Rossby-number limit – and on horizontal scales larger than the equal depths of the two layers; see Ref. (2, 3) for more details on the derivation of QG. At leading order in Rossby number the vertical momentum equation reduces to hydrostatic balance*, while the horizontal flow is in geostrophic balance†. These two balances imply that both the flow field and the local thickness of each layer can be expressed in terms of the corresponding streamfunctions, $\psi_1(x, y, t)$ in the upper layer and $\psi_2(x, y, t)$ in the lower layer. At the next order in Rossby number, the vertical vorticity equation yields the evolution equations for 32 33 34 35 36 37 38 39 40 41 42 43

*Hydrostatic balance is the balance between the upward-directed pressure gradient force and the downward-directed force of gravity.

†Geostrophic balance is the balance between the Coriolis force and lateral pressure gradient forces.

Significance Statement

Developing a theory of climate requires an accurate parameterization of the transport induced by turbulent eddies. A major source of turbulence in the mid-latitude planetary atmospheres and oceans is the baroclinic instability of the large-scale flows. We present a scaling theory that quantitatively predicts the local heat flux, eddy kinetic energy and mixing length of baroclinic turbulence as a function of the large-scale flow characteristics and bottom friction. The theory is then used as a quantitative parameterization in the case of meridionally dependent forcing, in the fully turbulent regime. Beyond its relevance for climate theories, our work is an intriguing example of a successful closure for a fully turbulent flow.

The authors declare no conflict of interest.

¹ All the authors contributed equally to this work.

² To whom correspondence should be addressed. E-mail: basile.gallet@cea.fr

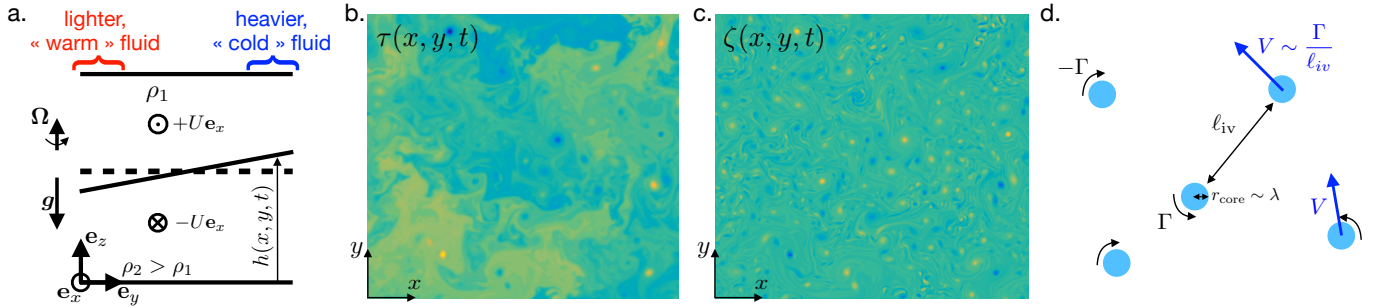


Fig. 1. panel a: base state of the 2LQG system with imposed vertical shear. The interface is tilted in the y direction as a consequence of thermal wind balance. The baroclinic streamfunction is proportional to $-h$, where $h(x, y, t)$ is the local displacement of the interface. For this reason, the baroclinic streamfunction is often referred to as the “temperature” field. Snapshots of the departure of the baroclinic streamfunction from the base state (τ , panel b) and of the barotropic vorticity (ζ , panel c) from a numerical simulation in the low-friction regime (arbitrary units, low values in dark blue and large values in bright yellow). We model the barotropic flow as a gas of vortices (panel d) of circulation $\pm\Gamma$ and radius $r_{\text{core}} \sim \lambda$. The vortex cores move as a result of their mutual interaction, with a typical velocity $V \sim \Gamma/\ell_{iv}$, where ℓ_{iv} is the typical inter-vortex distance.

44 $\psi_1(x, y, t)$ and $\psi_2(x, y, t)$:

45
$$\partial_t q_1 + J(\psi_1, q_1) = -\nu \Delta^4 q_1, \quad [1]$$

46
$$\partial_t q_2 + J(\psi_2, q_2) = -\nu \Delta^4 q_2 + \text{drag}, \quad [2]$$

47 where the subscripts 1 and 2 refer again to the upper and
 48 lower layers, and the Jacobian is $J(f, g) = \partial_x f \partial_y g - \partial_x g \partial_y f$.
 49 The potential vorticities $q_1(x, y, t)$ and $q_2(x, y, t)$ are related
 50 to the streamfunctions through:

51
$$q_1 = \nabla^2 \psi_1 + \frac{1}{2\lambda^2} (\psi_2 - \psi_1), \quad [3]$$

52
$$q_2 = \nabla^2 \psi_2 + \frac{1}{2\lambda^2} (\psi_1 - \psi_2), \quad [4]$$

53 where λ denotes the Rossby deformation radius[‡]. In
 54 our model, the drag term is confined to the lower-layer
 55 equation [2]. In the case of linear drag, $\text{drag} =$
 56 $-2\kappa \nabla^2 \psi_2$, and in the case of quadratic drag, $\text{drag} =$
 57 $-\mu [\partial_x (|\nabla \psi_2|^2 \partial_x \psi_2) + \partial_y (|\nabla \psi_2|^2 \partial_y \psi_2)]$. Finally, equations [1]
 58 and [2] include hyperviscosity to dissipate filaments of poten-
 59 tial vorticity (enstrophy) generated by eddy stirring at small
 60 scales.

61 A more insightful representation arises from the sum and
 62 difference of equations [1] and [2]: one obtains an evolution
 63 equation for the barotropic streamfunction – half the sum of
 64 the streamfunctions of both layers – which characterizes the
 65 vertically invariant part of the flow, and an evolution equation
 66 for the baroclinic streamfunction – half the difference between
 67 the two streamfunctions – which characterizes the vertically
 68 dependent flow. Because in QG the streamfunction is directly
 69 proportional to the thickness of the fluid layer, the baroclinic
 70 streamfunction is also a measure of the height of the inter-
 71 face between the two layers. A region with large baroclinic
 72 streamfunction corresponds to a locally deeper upper layer:
 73 there is more light fluid at this location, and we may thus say
 74 that on vertical average the fluid is warmer. Similarly, a re-
 75 gion of low baroclinic streamfunction corresponds to a locally
 76 shallower upper layer, with more heavy fluid: this is a cold
 77 region. Thus, the baroclinic streamfunction is often denoted
 78 as τ and referred to as the local “temperature” of the fluid.

79 The 2LQG model can be used to study the equilibration
 80 of baroclinic instability arising from a prescribed horizontally

uniform vertical shear, which represents the large-scale flows
 maintained by external forcing in the ocean and atmosphere.
 Denoting the vertical axis as z and the zonal and meridional
 directions as x and y , the prescribed flow in the upper
 and lower layers consists respectively in zonal motion $+U\mathbf{e}_x$
 and $-U\mathbf{e}_x$. This flow is in thermal wind balance[§] with a
 prescribed uniform meridional temperature gradient $-U$, i.e.
 there is a sloping interface between the heavy and light fluid
 layers, see Fig. 1a. This tilt provides an energy reservoir,
 the Available Potential Energy (APE, 4), that is released by
 baroclinic instability acting to flatten the density interface.
 We denote respectively as $\psi(x, y, t)$ and $\tau(x, y, t)$ the per-
 turbations of barotropic and baroclinic streamfunctions around
 this base state, and consider their evolution equations inside a
 large (horizontal) domain with periodic boundary conditions
 in both x and y :

97
$$\partial_t (\nabla^2 \psi) + J(\psi, \nabla^2 \psi) + J(\tau, \nabla^2 \tau) + U \partial_x (\nabla^2 \tau) \quad [5]$$

98
$$= -\nu \nabla^{10} \psi + \text{drag}/2,$$

99
$$\partial_t [\nabla^2 \tau - \lambda^{-2} \tau] + J(\psi, \nabla^2 \tau - \lambda^{-2} \tau) + J(\tau, \nabla^2 \psi) \quad [6]$$

100
$$+ U \partial_x [\nabla^2 \psi + \lambda^{-2} \psi] = -\nu \nabla^8 [\nabla^2 \tau - \lambda^{-2} \tau] - \text{drag}/2.$$

101 The system releases APE by developing eddy motion through
 102 baroclinic instability, and the goal is to characterize the statis-
 103 tically steady turbulent state that ensues: how energetic is the
 104 barotropic flow? How strong are the local temperature fluc-
 105 tuations? And, most importantly, what is the eddy-induced
 106 meridional heat-flux? The latter quantity is a key missing
 107 ingredient required to formulate a theory of the mean state
 108 of the atmosphere and ocean as a function of external forcing
 109 parameters (5).

110 Traditionally, these questions have been addressed using
 111 descriptions of the flow in spectral space, focusing on the
 112 cascading behavior of the various invariants (6). In contrast
 113 with this approach, Thompson & Young (7, TY in the fol-
 114 lowing) describe the system in physical space and argue that
 115 the barotropic flow evolves towards a gas of isolated vortices.
 116 In spite of this intuition, TY cannot conclude on the scal-
 117 ing behavior of the quantities mentioned above and resort to
 118 empirical fits instead. Focusing on the case of linear drag,
 119 they conclude that the temperature fluctuations and merid-
 120 ional heat flux are extremely sensitive to the drag coefficient:

[‡]The Rossby radius of deformation λ is the length scale at which rotational effects become as important as buoyancy or gravity wave effects in the evolution of a flow.

[§]A flow is in thermal wind balance if frictional forces and accelerations are weak, except for the Coriolis acceleration associated with Earth’s rotation.

121 they scale exponentially in inverse drag coefficient. This scal- 181
 122 ing dependence was recently shown by Chang & Held (8, CH 182
 123 in the following) to change quite drastically if linear drag is 183
 124 replaced by quadratic drag: the exponential dependence 184
 125 becomes a power-law dependence on the drag coefficient. How- 185
 126 ever, CH acknowledge the failure of standard cascade argu- 186
 127 ments to predict the exponents of these power laws, and they 187
 128 resort to curve fitting as well. 188

129 In this Letter, we supplement the vortex gas approach of 189
 130 TY with statistical arguments from point vortex dynamics to 190
 131 obtain a predictive scaling theory for the eddy kinetic energy, 191
 132 the temperature fluctuations and the meridional heat flux of 192
 133 baroclinic turbulence. The resulting scaling theory captures 193
 134 both the exponential dependence of these quantities on the in- 194
 135 verse linear drag coefficient, and their power-law dependence 195
 136 on the quadratic drag coefficient. Our predictions are thus 196
 137 in quantitative agreement with the scaling-laws diagnosed by 197
 138 both TY and CH. Following Pavan & Held (9) and CH, we 198
 139 finally show how these scaling-laws can be used as a quantita- 199
 140 tive turbulent closure to make analytical predictions in situ- 200
 141 ations where the system is subject to inhomogeneous forcing 201
 142 at large scale. 202

143 The QG vortex gas

144 Denoting as $\langle \cdot \rangle$ a spatial and time average and as $\psi_x = \partial_x \psi$ 203
 145 the meridional barotropic velocity, our goal is to determine 204
 146 the meridional heat flux $\langle \psi_x \tau \rangle$, or equivalently the diffusiv- 205
 147 ity $D = \langle \psi_x \tau \rangle / U$ that connects this heat flux to minus the 206
 148 background temperature gradient U . A related quantity of in- 207
 149 terest is the mixing-length $\ell = \sqrt{\langle \tau^2 \rangle} / U$. This is the typical 208
 150 distance travelled by a fluid element carrying its background 209
 151 temperature, before it is mixed with the environment and re- 210
 152 laxes to the local background temperature. It follows that 211
 153 the typical temperature fluctuations around the background 212
 154 gradient are of the order of $U\ell$. We seek the dependence of 213
 155 D and ℓ on the various external parameters of the system. It 214
 156 was established by TY that, for a sufficiently large domain, 215
 157 the mixing-length saturates at a value much smaller than the 216
 158 domain size, and independent of it. The consequence is that 217
 159 the size of the domain is irrelevant for large enough domains. 218
 160 The small-scale dissipation coefficient – a hyperviscosity in 219
 161 most studies – is also shown by TY to be irrelevant when 220
 162 low enough. The quantities D and ℓ thus depend only on the 221
 163 dimensional parameters U , the Rossby deformation radius λ , 222
 164 and the bottom drag coefficient, denoted as κ in the case of 223
 165 linear friction (with dimension of an inverse time) and as μ 224
 166 in the case of quadratic drag (with dimension of an inverse 225
 167 length) (8, 10). In dimensionless form, we thus seek the de- 226
 168 pendence of the dimensionless diffusivity $D_* = D/U\lambda$ and 227
 169 mixing-length $\ell_* = \ell/\lambda$ on the dimensionless drag $\kappa_* = \kappa\lambda/U$ 228
 170 or $\mu_* = \mu\lambda$. 229

171 We follow the key intuition of TY that the flow is better 230
 172 described in physical space than in spectral space. In Fig. 1, 231
 173 we provide snapshots of the barotropic vorticity and baro- 232
 174 clinic streamfunction from a direct numerical simulation in 233
 175 the low-drag regime (see the numerical methods in the Sup- 234
 176 plementary Information, SI): the barotropic flow consists of a 235
 177 “gas” of well-defined vortices, with a core radius substantially 236
 178 smaller than the inter-vortex distance ℓ_{iv} . Vortex gas models 237
 179 were introduced to describe decaying two-dimensional (purely 238
 180 barotropic) turbulence. It was shown that the time evolution 239

of the gross vortex statistics, such as the typical vortex radius 181
 and circulation, can be captured using simpler “punctuated 182
 Hamiltonian” models (11–13). The latter consist in integrat- 183
 ing the Hamiltonian dynamics governing the interaction of 184
 localized compact vortices (14), interrupted by instantaneous 185
 merging events when two vortices come close enough to one 186
 another, with specific merging rules governing the strength 187
 and radius of the vortex resulting from the merger. These 188
 models were adapted to the forced-dissipative situation by 189
 Weiss (15), through injection of small vortices with a core 190
 radius comparable to the injection scale, and removal of the 191
 largest vortices above a cut-off vortex radius. The resulting 192
 model captures the statistically steady distribution of vortex 193
 core radius observed in direct numerical simulations of the 2D 194
 Navier-Stokes equations (16): $P(r_{\text{core}}) \sim r_{\text{core}}^{-4}$ for r_{core} 195
 above the injection scale. One immediate consequence of such a 196
 steeply decreasing distribution function is that the mean vortex 197
 core radius is comparable to the injection scale. Similarly, 198
 the average vortex circulation is dominated by the circulation 199
 of the injected vortices. In the following, we will thus infer 200
 the transport properties of the barotropic component of the 201
 two-layer model by focusing on an idealised vortex gas consist- 202
 ing of vortices with a single “typical” value of the vortex 203
 core radius r_{core} comparable to the injection scale, and circula- 204
 tions $\pm\Gamma$, where Γ is the typical magnitude of the vortex 205
 circulation. For baroclinic turbulence, both linear stability 206
 analysis (2, 3) and the multiple cascade picture (6) indicate 207
 that the barotropic flow receives energy at a scale comparable 208
 to the deformation radius λ . As discussed above, the typical 209
 vortex core radius is comparable to this injection scale, and 210
 we obtain $r_{\text{core}} \sim \lambda$. We stress the fact that such a small core 211
 radius is fully compatible with the phenomenology of the in- 212
 verse energy cascade: inverse energy transfers result in the 213
 vortices being further apart, with little increase in core radi- 214
 us. The resulting velocity structures have a scale compar- 215
 able to the large inter-vortex distance, even though the intense 216
 vortices visible in the vorticity field have a small core radius, 217
 comparable to the injection scale. Finally, it is worth noting 218
 that there is encouraging observational evidence both in the 219
 atmosphere and ocean that eddies have a core radius close 220
 to the scale at which they are generated through baroclinic 221
 instability (17, 18). 222

223 A schematic of the resulting idealized vortex gas is pro- 224
 225 vided in Fig. 1d: we represent the barotropic flow as a collec- 226
 227 tion of vortices of circulation $\pm\Gamma$ and of core radius $r_{\text{core}} \sim \lambda$, 228
 229 and thus a velocity decaying as $\pm\Gamma/r$ outside the core (19). 230
 The vortices move as a result of their mutual interactions, 231
 with a typical velocity $V \sim \Gamma/\ell_{iv}$. Through this vortex gas 232
 picture, we have introduced two additional parameters, ℓ_{iv} 233
 and V – or, alternatively, $\Gamma = \ell_{iv} V$ – for a total of five pa- 234
 rameters: D , ℓ , ℓ_{iv} , V , and a drag coefficient (κ or μ). We thus 235
 need four relations between these five quantities to produce a 236
 fully closed scaling theory. 237

238 The first of these relations is the energy budget: the 239
 240 meridional heat flux corresponds to a rate of release of APE, 241
 242 $U \langle \psi_x \tau \rangle / \lambda^2 = DU^2 / \lambda^2$, which is balanced by frictional dissi- 243
 244 pation of kinetic energy in statistically steady state. The con- 244
 245 tribution from the barotropic flow dominates this frictional 245
 246 dissipation in the low-drag asymptotic limit, and the energy 246
 247 budget is 247
 248 $DU^2 / \lambda^2 = \kappa U^2 \ell_{iv}^2$ 248
 249 or 249

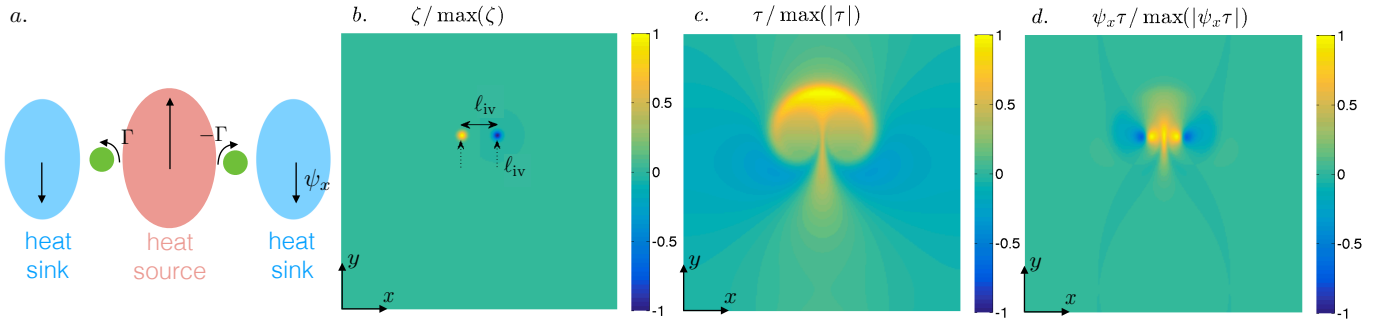


Fig. 2. Heat transport by a barotropic vortex dipole. Panel a is a schematic representation of the heat sources and sinks induced by the dipolar velocity field. Panels b, c and d show respectively the barotropic vorticity, temperature field, and local meridional heat flux, at the end time of a numerical solution of [10] where the dipole travels over a distance ℓ_{iv} in the meridional direction y .

power integral reads (see e.g. TY, and the SI):

$$\frac{DU^2}{\lambda^2} = \begin{cases} \kappa \langle \mathbf{u}^2 \rangle & \text{for linear drag,} \\ \frac{\mu}{2} \langle |\mathbf{u}|^3 \rangle & \text{for quadratic drag,} \end{cases} \quad [7]$$

where $\mathbf{u} = -\nabla \times (\psi \mathbf{e}_z)$ denotes the barotropic velocity field. Our approach departs from both TY and CH in the way we evaluate the velocity statistics that appear on the right-hand side: we argue that a key aspect of vortex gas dynamics is that the various velocity moments scale differently, and cannot be estimated simply as V above. Indeed, consider a single vortex within the vortex gas. It occupies a region of the fluid domain of typical extent ℓ_{iv} . The vorticity is contained inside a core of radius $r_{core} \sim \lambda \ll \ell_{iv}$, and the barotropic velocity \mathbf{u} has a magnitude $\Gamma/2\pi r$ outside the vortex core, where r is the distance to the vortex center. The velocity variance is thus:

$$\langle \mathbf{u}^2 \rangle = \frac{1}{\pi \ell_{iv}^2} \int_{r_{core}}^{\ell_{iv}} \frac{\Gamma^2}{4\pi^2 r^2} 2\pi r dr \sim V^2 \log\left(\frac{\ell_{iv}}{\lambda}\right). \quad [8]$$

This estimate for $\langle \mathbf{u}^2 \rangle$ exceeds that of TY by a logarithmic correction that captures the fact that the velocity is strongest close to the core of the vortex. This correction will turn out to be crucial to obtain the right scaling behaviors for D_* and ℓ_* . In a similar fashion, we estimate the third-order moment of the barotropic velocity field as:

$$\langle |\mathbf{u}|^3 \rangle = \frac{1}{\pi \ell_{iv}^2} \int_{r_{core}}^{\ell_{iv}} \frac{\Gamma^3}{8\pi^3 r^3} 2\pi r dr \sim V^3 \frac{\ell_{iv}}{\lambda}, \quad [9]$$

where we have used the fact that $r_{core} \sim \lambda \ll \ell_{iv}$. Again, this estimate exceeds that of CH by the factor ℓ_{iv}/λ , a correction that arises from the vortex gas nature of the flow field.

The next steps of the scaling theory are common to linear and quadratic drag. As in any mixing-length theory, we will express the diffusion coefficient D as the product of the mixing-length and a typical velocity scale. In the vortex gas regime, one can anticipate that the mixing-length ℓ scales as the typical inter-vortex distance ℓ_{iv} , an intuition that will be confirmed by equation [11] below. However, a final relationship for the relevant velocity scale is more difficult to anticipate, as we have seen that the various barotropic velocity moments scale differently. The goal is thus to determine this velocity scale through a precise description of the transport properties of the assembly of vortices.

Stirring of a tracer like temperature takes place at scales larger than the stirring rods, in our problem the vortices of

size λ . At scales much larger than λ , the τ equation [6] reduces to (7, 20, 21):

$$\partial_t \tau + J(\psi, \tau) = U \psi_x - \nu \Delta^4 \tau. \quad [10]$$

$U \psi_x$ represents the generation of τ -fluctuations through stirring of the large-scale temperature gradient $-U$, and the Jacobian term represents the advection of τ -fluctuations by the barotropic flow. Equation [10] is thus that of a passive scalar with an externally imposed uniform gradient $-U$ stirred by the barotropic flow. To check the validity of this analogy, we have implemented such passive-tracer dynamics into our numerical simulations: in addition to solving equations [5] and [6], we solve equation [10] with τ replaced by the concentration c of a passive scalar, and $-U$ replaced by an imposed meridional gradient $-G_c$ of scalar concentration. In the low-drag simulations, the resulting passive scalar diffusivity $D_c = \langle \psi_x c \rangle / G_c$ equals the temperature diffusivity D within a few percents, whereas D is significantly lower than D_c for larger drag, when the inter-vortex distance becomes comparable to λ . This validates our assumption that the diffusivity is mostly due to flow structures larger than λ in the low-drag regime, whose impact on the temperature field is accurately captured by the approximate equation [10]. We can thus safely build intuition into the behavior of the temperature field by studying equation [10].

A natural first step would be to compute the heat flux associated with a single steady vortex. However, this situation turns out to be rather trivial: the vortex stirs the temperature field along closed circles until it settles in a steady state that has a vanishing projection onto the source term $U \psi_x$, and the resulting heat flux $\langle \psi_x \tau \rangle$ vanishes up to hyperviscous corrections. Instead of a single steady vortex, the simplest heat carrying configuration is a vortex dipole, such as the one sketched in Fig. 2a: two vortices of opposite circulations $\pm \Gamma$ are separated by a distance ℓ_{iv} much larger than their core radius $r_{core} \sim \lambda$. This dipole mimics the two nearest vortices of any given fluid element, which we argue is a sufficient model to capture the qualitative transport properties of the entire vortex gas. Without loss of generality, the vortices are initially aligned along the zonal axis, and, as a result of their mutual interaction, they travel in the y direction at constant velocity $\Gamma/2\pi \ell_{iv}$. For the configuration sketched in Fig. 2a the meridional velocity is positive between the two vortices and becomes negative at both ends of the dipole. For positive U , this corresponds to a heat source between the vortices,

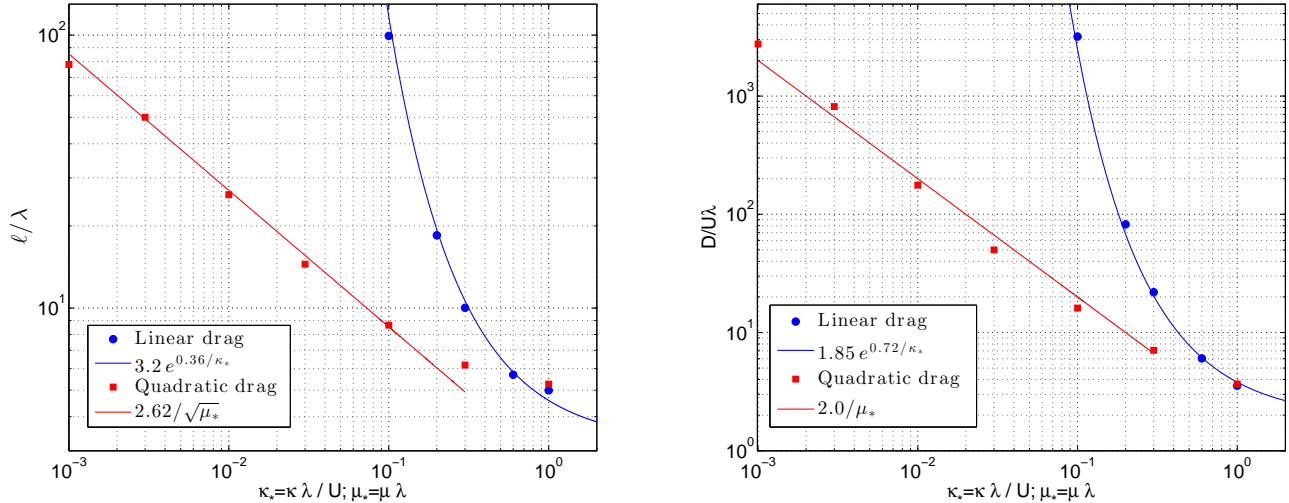


Fig. 3. Dimensionless mixing length ℓ_* and diffusivity D_* as functions of dimensionless drag, for both linear and quadratic drag. Symbols correspond to numerical simulations, while the solid lines are the predictions [15], [16], [17] and [18] from the vortex gas scaling theory.

322 and two heat sinks away from the dipole. These heat sources
 323 and sinks are positively correlated with the local meridional
 324 barotropic velocity, so that there is a net meridional heat flux
 325 $\langle \psi_x \tau \rangle$ associated with this configuration. We have integrated
 326 numerically equation [10] for this moving dipole, over a time
 327 ℓ_{iv}/V , which corresponds to the time needed for the dipole to
 328 travel a distance ℓ_{iv} . This is the typical distance travelled by
 329 these two vortices before pairing up with other vortices inside
 330 the gas. Panels 2c,d show the resulting temperature field and
 331 local flux $\psi_x \tau$ at the end of the numerical integration (see
 332 the SI for details). A suite of numerical simulations for such
 333 dipole configurations indicates that, at the end time of the
 334 numerical integration, the local mixing length and diffusivity
 335 obey the scaling relations:

$$336 \quad \ell \sim \ell_{iv}, \quad [11]$$

$$337 \quad D \sim \ell_{iv} V, \quad [12]$$

338 while the variance and third-order moment of the vortex
 339 dipole flow field satisfy [8] and [9] at every time. It is in-
 340 teresting that the velocity scale arising in the diffusivity [12]
 341 is V and not the rms velocity $\langle \mathbf{u}^2 \rangle^{1/2}$. This is because the
 342 fluid elements that are trapped in the immediate vicinity of
 343 the vortex cores do not carry heat, in a similar fashion that a
 344 single vortex is unable to transport heat. Only the fluid ele-
 345 ments located at a fraction of ℓ_{iv} away from the vortex centers
 346 carry heat, and these fluid elements have a typical velocity V .

347 The relations [11] and [12] hold for any passive tracer. How-
 348 ever, temperature is an active tracer, so that the velocity
 349 scale in-turn depends on the temperature fluctuations, pro-
 350 viding the fourth scaling relation. This relation can be de-
 351 rived through a simple heuristic argument: consider a fluid
 352 particle, initially at rest, that accelerates in the meridional

direction by transforming potential energy into barotropic ki- 353
 netic energy by flattening the density interface as a result of 354
 baroclinic instability. In line with the standard assumptions 355
 of a mixing-length model, we assume that the fluid particle 356
 travels in the meridional direction over a distance ℓ , before in- 357
 teracting with the other fluid particles. Balancing the kinetic 358
 energy gained over the distance ℓ with the difference in po- 359
 tential energy between two fluid columns a distance ℓ apart, 360
 we obtain the final barotropic velocity of the fluid element: 361
 $v_f \sim U\ell/\lambda$. This velocity estimate does not hold for the 362
 particles that rapidly loop around a vortex center, with little 363
 changes in APE; it holds only for the fluid elements that travel 364
 in the meridional direction, following a somewhat straight tra- 365
 jectory (these fluid elements happen to be the ones that carry 366
 heat, according to the dipole model described above). Such 367
 fluid elements have a typical velocity V , which we identify 368
 with v_f to obtain: 369

$$370 \quad V \sim U\ell/\lambda. \quad [13]$$

A similar relation was derived by Green (22), who computes 371
 the kinetic energy gained by flattening the density interface 372
 over the whole domain. In the present periodic setup the 373
 mean slope of the interface is imposed, and the estimate [13] 374
 holds locally for the heat-carrying fluid elements travelling a 375
 distance ℓ instead. The estimate [13] is also reminiscent of 376
 the “free-fall” velocity estimate of standard upright convec- 377
 tion, where the velocity scale is estimated as the velocity ac- 378
 quired during a free-fall over one mixing-length (23–25). The 379
 conclusion is that the typical velocity is directly proportional 380
 to the mixing length. The baroclinic instability is sometimes 381
 referred to as slant-wise convection, and the velocity estimate 382
 [13] is the corresponding “slant-wise free fall” velocity. To val- 383
 idate [13], one can notice that, when combined with [11] and 384

385 [12], it leads to the simple relation:

$$386 \quad D_* \sim \ell_*^2. \quad [14]$$

387 Anticipating the numerical results presented in Fig. 3, this relation is well satisfied in the dilute low-drag regime, $\ell \gtrsim 10\lambda$,
 388 the solid lines in both panels being precisely related by [14]
 389 above. A relation very close to [14] was reported by Larichev
 390 & Held using turbulent-cascade arguments (21). Their relation
 391 is written in terms of an “energy containing wavenumber”
 392 instead of a mixing-length. If this energy containing wavenumber
 393 is interpreted to be the inverse inter-vortex distance of
 394 the vortex-gas model, then their relation becomes identical to
 395 [14].
 396

397 The four relations needed to establish the scaling theory
 398 are [7], [11], [12] and [13]. In the case of linear drag, their
 399 combination leads to $\log(\ell_*) \sim 1/\kappa_*$, or simply:

$$400 \quad \ell_* = c_1 \exp\left(\frac{c_2}{\kappa_*}\right), \quad [15]$$

401 where c_1 and c_2 are dimensionless constants. The vortex gas
 402 approach thus provides a clear theoretical explanation to the
 403 exponential dependence of ℓ on inverse drag reported by TY,
 404 which is shown to stem from the logarithmic factor in [8] for
 405 the dissipation of kinetic energy. It is remarkable that these
 406 authors could extract the correct functional dependence of ℓ_*
 407 with κ_* from their numerical simulations. We have performed
 408 similar numerical simulations, in large enough domains to
 409 avoid finite-size effects, and at low enough hyperviscosity to
 410 neglect hyperdissipation in the kinetic energy budget. The
 411 numerical implementation of the equations, as well as the parameter
 412 values of the various numerical runs, are provided in
 413 the SI. In Fig. 3, we plot ℓ_* as a function of κ_* . We obtain an
 414 excellent agreement between the asymptotic prediction [15]
 415 and our numerical data using $c_1 = 3.2$ and $c_2 = 0.36$. The
 416 dimensionless diffusivity is deduced from ℓ_* using the relation
 417 [14], which leads to:

$$418 \quad D_* = c_3 \exp\left(\frac{2c_2}{\kappa_*}\right). \quad [16]$$

419 Once again, upon choosing $c_3 = 1.85$ this expression is in
 420 excellent agreement with the numerical data, see Fig. 3.

421 When linear friction is replaced by quadratic drag, only
 422 the energy budget [7] is modified. As can be seen in equation
 423 [9], the main difference is that quadratic drag operates
 424 predominantly in the vicinity of the vortex cores, which has a
 425 direct impact on the scaling behaviors of ℓ_* and D_* . Indeed,
 426 combining [7], [11], [12] and [13] yields:

$$427 \quad \ell_* = \frac{c_4}{\sqrt{\mu_*}}, \quad [17]$$

428 which, using [14], leads to the diffusivity:

$$429 \quad D_* = \frac{c_5}{\mu_*}. \quad [18]$$

430 Using the values $c_4 = 2.62$ and $c_5 = 2.0$, the predictions
 431 are again in very good agreement with the numerical data,
 432 although the convergence to the asymptotic prediction for D_*
 433 seems somewhat slower for this configuration, see Fig. 3.

Using these scaling-laws as a local closure

434 We now wish to demonstrate the skill of these scaling-laws
 435 as local diffusive closures in situations where the heat-flux
 436 and the temperature gradient have some meridional variations.
 437 For simplicity, we consider an imposed heat flux with
 438 a sinusoidal dependence in the meridional direction y . The
 439 modified governing equations for the potential vorticities $q_{1,2}$
 440 of each layer are:

$$441 \quad \partial_t q_1 + J(\psi_1, q_1) = Q \sin(y/L) - \nu \Delta^4 q_1, \quad [19]$$

$$442 \quad \partial_t q_2 + J(\psi_2, q_2) = -Q \sin(y/L) - \nu \Delta^4 q_2 + \text{drag}. \quad [20]$$

443 It becomes apparent that the Q -terms represent a heat flux
 444 when the governing equations are written for the (total) baroclinic
 445 and barotropic streamfunctions τ and ψ : the τ -equation,
 446 obtained by subtracting [20] from [19] and dividing by two,
 447 has a source term $Q \sin(y/L)$ that forces some meridional temperature
 448 structure. By contrast, the ψ -equation obtained by adding [19]
 449 and [20] has no source terms. The goal is to determine the temperature
 450 profile associated with the imposed meridionally dependent heat flux.
 451 This slantwise convection forced by sources and sinks is somewhat
 452 similar to standard upright convection forced by sources and sinks
 453 of heat (26, 27). We focus on the statistically steady state by
 454 considering a zonal and time average, denoted as $\bar{\cdot}$. Neglecting the
 455 dissipative terms, the average of both equations [19] and [20] leads
 456 to:
 457

$$458 \quad Q \sin(y/L) = -\frac{1}{\lambda^2} \partial_y \overline{\psi_x \tau}. \quad [21]$$

459 Provided the imposed heat flux varies on a scale L much larger
 460 than the local mixing-length ℓ , we can relate the local flux
 461 $\overline{\psi_x \tau}(y)$ to the local temperature gradient $U(y) = \partial_y \bar{\tau}$ by the
 462 diffusive relation $\overline{\psi_x \tau}(y) = DU(y) = D_* \lambda |U(y)|U(y)$. In the
 463 case of quadratic drag, inserting this relation into [21] and
 464 substituting the scaling-law [18] for $D_*(\mu_*)$ yields:

$$465 \quad -\frac{c_5}{\mu_*} \partial_y [|\partial_y \bar{\tau}| \partial_y \bar{\tau}] = Q \sin(y/L). \quad [22]$$

466 In terms of the dimensionless temperature $\tau_* = \tau/\lambda^2 \sqrt{Q}$, the
 467 solution to this equation is:

$$468 \quad \bar{\tau}_*(y/L) = 2 \left(\frac{L}{\lambda}\right)^{3/2} \sqrt{\frac{\mu_*}{c_5}} \mathcal{E}\left(\frac{y}{L} | 2\right), \quad [23]$$

469 where \mathcal{E} denotes the incomplete elliptic integral of the second
 470 kind. Expression [23] holds for $y/L \in [-\pi/2; \pi/2]$, the entire
 471 graph being easily deduced from the fact that $\bar{\tau}_*(y/L)$ is symmetric
 472 to a translation by π accompanied by a sign change.
 473

474 In the case of linear drag, we substitute the scaling-law [16]
 475 for $D_*(\kappa_*) = D_*(\lambda \kappa_*/|\partial_y \bar{\tau}|)$ instead. The integration of the
 476 resulting ODE yields the dimensionless temperature profile:

$$477 \quad \bar{\tau}_*(y/L) = \frac{\kappa L}{c_2 \lambda \sqrt{Q}} \int_0^{y/L} \mathcal{W}\left(\frac{c_2}{\kappa} \sqrt{\frac{LQ}{c_3 \lambda}} \cos s\right) ds, \quad [24]$$

478 where \mathcal{W} denotes the Lambert function. Once again, [24]
 479 holds for $y/L \in [-\pi/2; \pi/2]$, the entire graph being easily deduced
 480 from the fact that $\bar{\tau}_*(y/L)$ is symmetric to a translation
 481 by π accompanied by a sign change.

482 To test these theoretical predictions, we solved numerically
 483 equations [19-20] inside a domain $(x, y) \in [0; 2\pi L]^2$ with

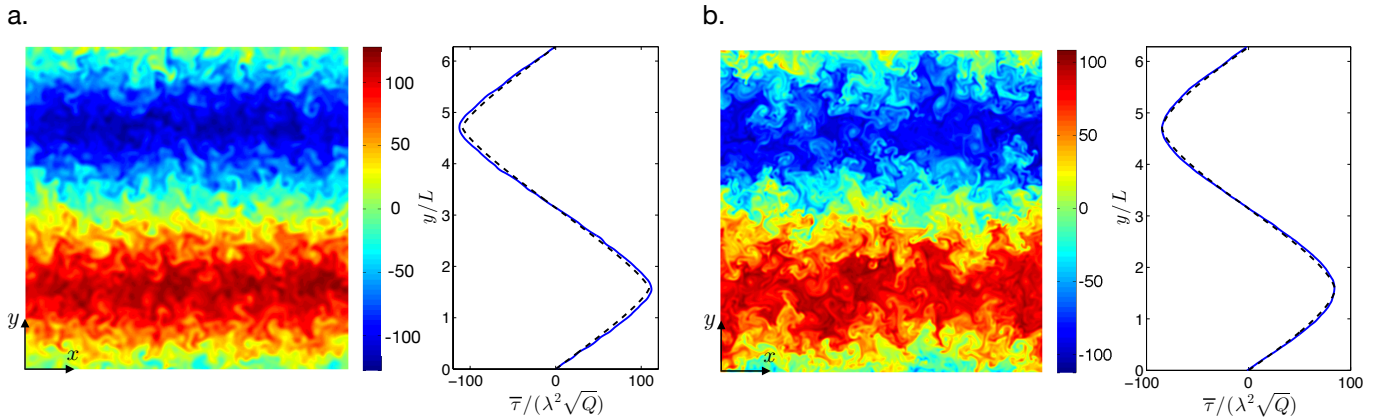


Fig. 4. Testing the diffusive closure. Snapshots and meridional profiles of the dimensionless temperature $\tau/\lambda^2 Q^{1/2}$. The solid lines are the zonal and time mean from the numerical simulations, while the dashed lines are the theoretical expressions [24] and [23]. a. Linear drag, with $\kappa/Q^{1/2} = 0.5$ and $\lambda/L = 0.02$. b. Quadratic drag, with $\mu_* = 10^{-2}$ and $\lambda/L = 0.01$.

484 periodic boundary conditions, for both linear and quadratic
 485 drag. We compute the time and zonally averaged tempera-
 486 ture profiles and compare them to the theoretical predictions,
 487 using the values of the parameters $c_{1;2;3;4;5}$ deduced above. In
 488 Fig. 4, we show snapshots of the temperature field in statisti-
 489 cally steady state, together with meridional temperature pro-
 490 files. The predictions [23] and [24] are in excellent agreement
 491 with the numerical results for both linear and quadratic drag,
 492 and this good agreement holds provided the various length
 493 scales of the problem are ordered in the following fashion:
 494 $\lambda \ll \ell \ll L$. The first inequality corresponds to the dilute
 495 vortex gas regime for which the scaling theory is established,
 496 while the second inequality is the scale separation required for
 497 any diffusive closure to hold. For fixed L/λ , the first inequal-
 498 ity breaks down at large friction, $\kappa_* \sim 1$ or $\mu_* \sim 1$, where
 499 the system becomes a closely packed “vortex liquid” (10, 28).
 500 The second inequality breaks down at low friction, when $\ell \sim L$.
 501 From the scaling-laws [15] and [17], this loss of scale separa-
 502 tion occurs for $\kappa_* \lesssim 1/\log(L/\lambda)$ and $\mu_* \lesssim (\lambda/L)^2$, respec-
 503 tively for linear and quadratic drag.

504 Discussion

505 The vortex gas description of baroclinic turbulence allowed
 506 us to derive predictive scaling-laws for the dependence of the
 507 mixing-length and diffusivity on bottom friction, and to cap-
 508 ture the key differences between linear and quadratic drag.
 509 The scaling behavior of the diffusivity of baroclinic turbu-
 510 lence appears more “universal” than that of its purely barotropic
 511 counterpart. This is likely because many different mechani-
 512 sms are used in the literature to drive purely barotropic
 513 turbulence. For instance, the power input by a steady sinu-
 514 soidal forcing (29, 30) strongly differs from that input by forc-
 515 ing with a finite (31) or vanishing (32) correlation time, with
 516 important consequences for the large-scale properties and dif-
 517 fusivity of the resulting flow. By contrast, baroclinic turbu-
 518 lence comes with its own injection mechanism – baroclinic in-
 519 stability – and the resulting scaling-laws depend only on the
 520 form of the drag. We demonstrated the skills of these scaling-
 521 laws when used as local parameterizations of the turbulent
 522 heat transport, in situations where the large-scale forcing is
 523 inhomogeneous. While this theory provides some qualitative
 524 understanding of turbulent heat transport in planetary at-

mospheres, it should be recognized that the scale separation is
 at best moderate in Earth atmosphere, where meridional
 changes in the Coriolis parameter also drive intense jets. On
 the other hand, our firmly footed scaling theory could be the
 starting point towards a complete parameterization of baro-
 clinic turbulence in the ocean, a much-needed ingredient of
 global ocean models. Along the path, one would need to
 adapt the present approach to models with multiple layers,
 possibly going all the way to a geostrophic model with con-
 tinuous density stratification, or even back to the primitive
 equations. The question would then be whether the vortex
 gas provides a good description of the equilibrated state in
 these more general settings. Even more challenging would be
 the need to include additional physical ingredients in the scal-
 ing theory: the meridional changes in f mentioned above, but
 also variations in bottom topography, and surface wind stress.
 Whether the vortex gas approach holds in those cases will be
 the topic of future studies.

Data availability. The data associated with this study are
 available within the paper and SI.

ACKNOWLEDGMENTS. Our work is supported by the generos-
 ity of Eric and Wendy Schmidt by recommendation of the Schmidt
 Futures program, and by the National Science Foundation under
 grant AGS-6939393. This research is also supported by the Eu-
 ropean Research Council (ERC) under grant agreement FLAVE
 757239.

1. G.R. Flierl, Models of vertical structure and the calibration of two-layer models, *Dyn. Atmos. Oceans* **2**, 342-381 (1978).
2. R. Salmon, Lectures on Geophysical Fluid Dynamics, *Oxford University Press* (1998).
3. G.K. Vallis, Atmospheric and oceanic fluid dynamics: fundamentals and large-scale circulation, *Cambridge University Press* (2006).
4. E.N. Lorenz, Available Potential Energy and the Maintenance of the General Circulation, *Tellus*, **7**, 157-167 (1955).
5. I.M. Held, The macroturbulence of the troposphere, *Tellus* **51A-B**, 59-70 (1999).
6. R. Salmon, Two-layer quasigeostrophic turbulence in a simple special case, *Geophys. Astrophys. Fluid Dyn.*, **10**, 25-52 (1978).
7. A.F. Thompson, W.R. Young, Scaling baroclinic eddy fluxes: vortices and energy balance, *J. Phys. Oceanogr.* **36**, 720-736 (2005).
8. C.-Y. Chang, I.M. Held, The control of surface friction on the scales of baroclinic eddies in a homogeneous quasigeostrophic two-layer model, *J. Atmospheric Sci.* **76**, 6 (2019).
9. V. Pavan, I.M. Held, The diffusive approximation for eddy fluxes in baroclinically unstable jets, *J. Atmospheric Sci.* **53**, 1262-1272 (1996).
10. B.K. Arbic, R.B. Scott, On quadratic bottom drag, geostrophic turbulence, and oceanic mesoscale eddies, *J. Phys. Oceanogr.* **38**, 84-103 (2007).
11. G.F. Carnevale, J.C. McWilliams, Y. Pomeau, J.B. Weiss, W.R. Young, Evolution of vortex statistics in two-dimensional turbulence, *Phys. Rev. Lett.* **66**, 2735-2737 (1991).

571 12. J.B. Weiss, J.C. McWilliams, Temporal scaling behavior of decaying two-dimensional turbulence, *Phys. Fluids A: Fluid Dynamics* **5**, 608 (1993).
572
573 13. E. Trizac, A coalescence model for freely decaying two-dimensional turbulence, *Europhys. Lett.* **43**, 671 (1998).
574
575 14. L. Onsager, Statistical Hydrodynamics, *Nuovo Cimento Suppl.*, **6**, 279, (1949).
576 15. J.B. Weiss, Punctuated Hamiltonian models of structured turbulence, in *Semi-Analytic Methods for the Navier-Stokes Equations*, CRM Proc. Lecture Notes, Amer. Math. Soc., **20**, 109-119, (1999).
577
578 16. V. Borue, Inverse energy cascade in stationary two-dimensional homogeneous turbulence, *Phys. Rev. Lett.* **72**, 10 (1994).
579
580 17. T. Schneider, C.C. Walker, Self-organization of atmospheric macroturbulence into critical states of weak nonlinear eddy-eddy interactions, *J. Atmospheric Sci.* **63**, 1569-1586 (2006).
581
582 18. R. Tulloch, J. Marshall, C. Hill, K.S. Smith, Scales, growth rates, and spectral fluxes of baroclinic instability in the ocean, *J. Phys. Oceanogr.* **41**, 6, 1057-1076 (2011).
583
584 19. J.G. Charney, Numerical experiments in atmospheric hydrodynamics, In: *Experimental Arithmetic, High Speed Computing and Mathematics, Proc. Symposia in Appl. Math.* **15**, 289-310 (1963).
585
586 20. R. Salmon, Baroclinic instability and geostrophic turbulence, *Geophys. Astrophys. Fluid Dyn.*, **15**, 157-211 (1980).
587
588 21. V. Larichev, I.M. Held, Eddy amplitudes and fluxes in a homogeneous model of fully developed baroclinic instability, *J. Phys. Oceanogr.* **25**, 2285-2297 (1995).
589
590 22. J.S.A. Green, Transfer properties of the large-scale eddies and the general circulation of the atmosphere, *Quart. J. R. Met. Soc.* **96**, 157-185 (1970).
591
592 23. E.A. Spiegel, A generalization of the mixing-length theory of thermal convection, *ApJ* **138**, 216 (1963).
593
594 24. E.A. Spiegel, Convection in stars I. Basic Boussinesq convection, *Annu. Rev. Astron. Astrophys.*, **9**, 323-352 (1971).
595
596 25. M. Gibert et al., High-Rayleigh-Number convection in a vertical channel, *Phys. Rev. Lett.* **96**, 084501 (2006).
597
598 26. S. Lepot, S. Aumaître, B. Gallet, Radiative heating achieves the ultimate regime of thermal convection, *Proc. Nat. Acad. Sci. U S A*, **115**, 36 (2018).
599
600 27. V. Bouillaut, S. Lepot, S. Aumaître, B. Gallet, Transition to the ultimate regime in a radiatively driven convection experiment, *J. Fluid Mech.*, **861**, R5 (2019).
601
602 28. B.K. Arbic, G.R. Flierl, Baroclinically unstable geostrophic turbulence in the limits of strong and weak bottom Ekman friction: application to midocean eddies, *J. Phys. Oceanogr.* **34**, 2257-2273 (2004).
603
604 29. Y.-K. Tsang, W.R. Young, Forced-dissipative two-dimensional turbulence: A scaling regime controlled by drag, *Phys. Rev. E*, **79**, 045308(R) (2009).
605
606 30. Y.-K. Tsang, Nonuniversal velocity probability densities in two-dimensional turbulence: The effect of large-scale dissipation, *Phys. Fluids*, **22**, 115102 (2010).
607
608 31. M.E. Maltrud, G.K. Vallis, Energy spectra and coherent structures in forced two-dimensional and beta-plane turbulence, *J. Fluid Mech.*, **228**, 321 (1991).
609
610 32. N. Gryanik, I.M. Held, K.S. Smith, G.K. Vallis, The effects of quadratic drag on the inverse cascade of two-dimensional turbulence, *Phys. Fluids*, **16**, 73 (2004).
611
612
613
614
615